Building and Environment 245 (2023) 110877

Contents lists available at ScienceDirect

Building and Environment

journal homepage: www.elsevier.com/locate/buildenv

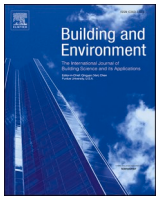

Current and future geographical distribution of the indoor conditions for high thermal inertia historic buildings across Portugal via hygrothermal simulation

Guilherme B.A. Coelho [a,*], Hugo B. Rebelo [b,c], Vasco Peixoto De Freitas [d], Fernando M. A. Henriques [c], Lourenço Sousa [c]

[a] Department of Built Environment, Faculty of Technology, Art and Design, Oslo Metropolitan University, PO box 4 St. Olavs plass, Oslo, NO-0130, Norway
[b] CINAMIL, Academia Militar, Instituto Universitário Militar, Rua Gomes Freire, 1169-203, Lisboa, Portugal
[c] CERIS, Departamento de Engenharia Civil, Faculdade de Ciências e Tecnologia, Universidade NOVA de Lisboa, Campus de Caparica, Caparica, 2829-516, Portugal
[d] CONSTRUCT-LFC, Faculty of Engineering, University of Porto, Portugal

ARTICLE INFO

Keywords:
Climate change
Historic buildings
Computational models
Multi-step mapping methodology
Mapping optimization
Indoor future conditions

ABSTRACT

Meteorological conditions play a major influence on the indoor conditions of buildings, especially in southern European countries, where the hygrothermal requirements are systematically neglected, on contrast to northern European countries. Outdoor conditions will greatly differ with a building's location, even more if climate change is considered. Designing or retrofitting should take the climate requirements and, if necessary, adapt appropriately.

This paper presents a methodology that can easily assess the variance of the indoor climate or even the performance of a retrofit measure in accordance with location. The methodology encompasses five steps: 1) *Set meteorological data*; 2) *Build outdoor weather files*; 3) *Obtain interface soil/slab temperature*; 4) *Obtain simulation outputs*; and 5) *Build map*. This methodology is flexible in terms of location/region, computational model, requirements and weather data.

A model of a historic church was used to compute current and future climates' distribution for Portugal. It was shown that the indoor climates are more moderate on locations near the coast than on those in the interior of the country, and that the buffering effect is higher in the west coast than in the south coast. A significant increase in terms of indoor temperature from scenario RCP 4.5 to RCP 8.5 is expected. In most of the coastal zones, an increase in RH is expected in the near future, whilst in some interior regions, a decrease is expected. Finally, it was shown that when using an adequate interpolation function, the coarser grid can correctly simulate the geographical distribution of the indoor conditions.

1. Introduction

A great number of buildings that house artefacts are historic buildings, which due to their very thick walls and low window/wall ratio are considered as high thermal inertia buildings [1]. This means that the variation of the indoor climate has a considerable time lag in correspondence with the variation of the outdoor conditions.

Due to these characteristics as well as the expected effects of climate change, it can be difficult to guarantee the proper indoor conditions for the preservation of artefacts – i.e. they do not suffer biological, chemical or mechanical decay [2,3]. When dealing with this type of buildings it is also necessary to take into account the building's occupants' thermal comfort [4] – either using an analytical model (e.g. Ref. [5]) or an adaptive model (e.g. Ref. [6]), and the building's energy consumption, which due to sustainability reasons, must be the lowest possible.

Modern passive retrofit measures, such as the replacement of the window systems or the application of a wall insulation system, are hard to implement in this type of buildings due to their heritage value [7] and the possible loss of authenticity [8]. In turn, this makes their indoor climate more prone to the effects of climate change [9], which makes both the building, as well as its content (e.g. artefacts) and its occupants (in terms of comfort), more prone to the effects of climate change.

* Corresponding author.
E-mail address: coelho@oslomet.no (G.B.A. Coelho).

https://doi.org/10.1016/j.buildenv.2023.110877
Received 12 June 2023; Received in revised form 12 September 2023; Accepted 24 September 2023
Available online 25 September 2023

Hence, it is of the utmost importance to determine how the indoor climate in this type of buildings is going to be in the future, so that the applied measures can have the greatest mitigation potential possible and, therefore, preserve the artefacts for future generations.

Due to the previously mentioned limitations imposed to modern interventions, their selection procedure must be based on a non-destructive method [10], such as, the two-step procedure of first monitor the indoor climate and then built computational calibrated models (e.g. Refs. [11,12]). This allows to perform "what-if scenarios" to choose the best-case scenario without inflicting unnecessary damage to the cultural heritage.

Climate change is one of the key challenges faced by mankind nowadays, since it will greatly influence the environment, human health and both global and local economy. Furthermore, these changes will also negatively affect the durability of buildings [13,14]. The effects of climate change will differ mainly according to how the world's energy consumption and the respective supply structure will evolve in the future, which can have great variability [15]. It is important to have the notion that the effects of climate change will differ in accordance with location [16]. This means that the recommended improvement measures should be fitted to the location of the case-study, thus taking into account the variation of the outdoor climate in the future for that location [17].

Due to the variability of all the factors that affect the emission of greenhouse gases (GHG) and, consequently, the outdoor climate, it is necessary to describe the different ways in which the outdoor climate might evolve. For this purpose, the *Intergovernmental Panel on Climate Change* (IPCC) developed several scenarios that are grounded on different assumptions. Their driving forces are the demographic and socio-economic developments, as well as the technological evolution and land use change [15].

The IPCC has reflected the expected changes that the outdoor climate will suffer by means of producing comprehensive assessment reports (ARs). Due to the need to reflect the updates suffered by climate change modelling, there is a need to produce new ARs periodically [15,18,19]. The future outdoor conditions that will be used in this study were determined in accordance with the scenarios of the 5th Assessment Report (AR5), named *Representative Concentration Pathway* (RCP). Nonetheless, the most recent report is the 6th assessment report [20], which was gradually published, starting August 2021, but its scenarios still have not been actively used in building science.

The RCPs describe four different ways in which the greenhouse gases, the air pollutants emissions, the atmospheric concentrations and the changes of land use can evolve in the future, namely [21]: RCP 2.6 (stringent mitigation scenario), RCP 4.5 and RCP 6.0 (two intermediate scenarios), RCP 8.5 (high GHGs emissions). Contrary to the previous *Special Report on Emission Scenarios* (SRES) scenarios [18], some of the RCPs' scenarios include future climate policies [22]. Whilst RCP 2.6 is a mitigation scenario that includes this sort of policies to reduce the GHGs emission; the RCP 6.0 and RCP 8.5 are baseline scenarios that do not include these policies, thus reaching a higher level of GHGs emissions [21].

The climate change projected by the RCPs' scenarios for Europe in terms of patterns and magnitude are the following [16]: 1) increase of the global temperature all over Europe, but to a bigger extent in southern Europe during the summer, as well as in northern Europe during the winter; 2) decrease of precipitation in southern Europe, and its increase in northern Europe; 3) increase in the number of heat waves, droughts and heavy precipitation events; 4) increase of the global mean sea level, as well as extreme sea level events (e.g. storms); and 5) slight increase of the extreme wind speed during winter in central and northern Europe, and its slight decrease in southern Europe.

Although the variance of the outdoor climate is more substantial when different regions of the world are compared, e.g. when the climate of an African country is compared with the climate of a European country, the geographical variation of the outdoor climate between different regions of Europe is also visible [23]. The Iberian Peninsula is expected to be one of the most affected regions of Europe with the increase of temperature in summer and the decrease of precipitation, among others [16]. However, the outdoor climate variance's magnitude and rate will also differ for each location [16], which means that the indoor climate of historic buildings will also differ [24].

An efficient way of visualizing data when assessing the variation of any parameter across a large zone (e.g. a country), is by building variation maps. This way of data visualization is a frequently used technique in several fields (e.g. Refs. [25–30]), even in the artefacts conservation field, since it allows to easily visualize a parameter distribution throughout the selected area, e.g. either inside a building [28] or across a region/country [30]. This type of data representation can be obtained by either using monitored data or simulated data, which will generate specific point-data depending on the selected grid. This will be then transformed into a distribution map by means of using, for example, a spatial interpolation method [28].

Several studies using this type of data visualization form can be found in literature, but the purpose of these maps or how they are built significantly varies with the study goals. For instance, a straight form of using this methodology is to have a distribution of the indoor conditions so that the quality of the indoor climate for occupants can be ensured, as was carried out by Choi et al. [28] and Yu et al. [25]. Although both studies use the distribution maps based on measured data to ensure indoor climate quality, Choi et al. [28] focusses their assessment in IEQ factors (i.e. PPD, CO_2, VOCs and $PM_{2.5}$), while Yu et al. [25] focusses on indoor temperature to limit the indoor occupancy. This methodology can also be used, for example, to assess the thermal comfort outside buildings [26]. None of the previously addressed studies consider climate change to perform their assessments [25–30].

This data visualization technique can also be coupled to simulation software to study a region/country behaviour, as it will be performed in this study. For example, a very interesting and complete study was carried out by Vandemeulebroucke et al. [27], who run an enormous set of 1D simulations to assess the degradation risk of masonry in the future by means of using "Climate-based analysis" and "Response-based analysis" indices. This work is carried out for 10 specific climates, i.e. one for each climate zone in Europe and the Mediterranean, focussing the assessment on the building elements. In contrast, Verichev et al. [29] and Rajput et al. [30] use a whole-building simulation tool but both focus on energy simulations, which are much quicker to run than hygrothermal simulations [31], as it will be performed in this study. Moreover, both studies assess the energy consumption without considering climate change. Rajput et al. [30] focusses in a zone of the city of Chicago and used 375 grid points to build their maps, while Verichev et al. [29] focusses on a much larger region of Chile using 680 grid points for map building.

This type of presenting data is not a novelty in this scientific area since, for example, Huijbregts et al. [32] and other authors (e.g. Refs. [9,33–35]), have already carried out similar representations. However, the data that is presented in these maps differs, as well as the adopted inputs, among other aspects. For instance, the TU/e team developed two interesting studies in which the variance of several parameters (such as, indoor conditions, artefacts' decay and energy consumption) are shown in maps [9,32]. These works and others of the same kind were carried out under the scope of the "Climate for Culture" project [36], in which they determined the future indoor climate of historic buildings across Europe to "plan more effectively mitigation and adaption measures at various levels" [36]. A coarser grid was used, but the study was based on different typologies of historic buildings, which is natural due to the size of the assessed area.

Both studies used a similar methodology, i.e. assess the future indoor conditions – obtained from a calibrated historic building model coupled with future outdoor files – using damage functions, which obtained similar conclusions [9,32]. Firstly, it is expected that artefacts are not safe from some sort of decay in any location in Europe, this means that

the decay risks will differ according to the location. Secondly, the chemical decay risk is low, and the risk of mechanical decay and biological decay is high for cold and humid climates; while for the warm and dry climates, the biological decay risk is low, and the risk of chemical and mechanical decay is more critical.

The main difference between these two studies resides on the origin of the weather files. Whilst Ref. [9] uses the weather data from 138 weather stations that is available on Meteonorm and then interpolates for all of Europe, Ref. [32] uses the weather data from A1B scenario for 468 locations in Europe, thus having a finer grid across Europe, and, consequently, more accurate results.

More recently, van Schijndel and Schellen [33] created a very complete methodology that aims to predict and map the energy demand in historic buildings across Europe whilst taking into account climate change. The methodology, as is explained by them, is a four-step procedure that includes the development of the following tools: 1) Future weather files; 2) Building simulation models; 3) Museums classification system; and 4) Outputs mapping presentation tool [33]. In order to make the study more comprehensive, sixteen different models were run, each with one of four quality of envelope (QoE) and one of four level of control (LoC) [33]. However, to make the study feasible, the simulations were run for 300 locations across Europe, which means a rather coarse grid, and the run models correspond to a room that is representative of historic buildings. This latter option has the drawback of not considering the whole building with its characteristics. Nonetheless, these two simplifications are understandable given that 16 models were run, which means a total of 4800 hygrothermal simulations.

This study aims to analyse the variance of the future indoor climate of high thermal inertia buildings in Portugal, one of the countries that composes the Iberian Peninsula. For this purpose, an original methodology to build maps that show the geographical distribution of the indoor conditions was developed. Due to its nature, this methodology is backed by several software, i.e. WUFI®Plus [31], EnergyPlus [37] and MATLAB/OCTAVE, depending on the used computer, i.e. MATLAB is used in computer 1 and OCTAVE is used in computers 2 (see subsection 2.3).

The future outdoor weather files were built using the methodology described in standard EN 15927-4 [38] and the global radiation was split in its direct and diffuse components using the *Skartveit and Olseth* model [39,40]. The future indoor conditions – temperature and relative humidity – were obtained running a calibrated computational model of a high thermal inertia building [31,37], which computes and outputs them, coupled to the developed weather files. Finally, the obtained results were assessed and presented in the form of maps.

The study described here also uses a calibrated whole-building computational model of a high thermal inertia historic building and RCP future weather files to develop the shown maps, but with a much finer grid to characterize the selected zone (i.e. 229 locations just for Portugal) when compared with the previously mentioned studies. This will allow to detect the most susceptible areas in Portugal to the effects of climate change.

In addition, the developed mapping tool is extremely adaptable and all the methodology presented in 2.3 runs automatically, which increases its efficiency and at the same time decreases the risk of human error, i.e. eliminates operations associated with monotonous work [41], e.g. inputting the weather file and soil/slab temperature for numerous simulations [17]. Finally, the grid points spacing was also analysed.

2. Methodology

2.1. Research questions and aims

This paper studies the geographical variance of the indoor climate – temperature and relative humidity – of historic buildings with high thermal inertia under current and future conditions to determine the building's performance under the climate changes. This will enable to determine the areas in Portugal most susceptible to the effects of climate change, and, therefore, implement proper changes fitted for each location to safeguard the indoor climate.

For this purpose, a multi-step algorithm was developed that, for the selected zone, builds the weather files for each of the grid's points, both for current and future conditions. An EnergyPlus model is run to obtain the soil/slab interface temperature and a WUFI®Plus model is run to obtain the indoor climate for each of the grid defined points.

The study is conducted using a computational model of a 13th-century church typical across Portugal. The geographical variance of each of the studied parameters – temperature and relative humidity – is presented in the form of maps, which were developed for free-floating indoor conditions: indoor air temperature in the near future and far future (subsection 3.1); and indoor air relative humidity in the near future and far future (subsection 3.2). The developed maps represent the variations for Portugal since it is part of one of Europe's regions that is expected to be mostly affect by climate change [17].

In addition, the grid size is also studied (subsection 3.3) to determine if it is possible to reduce computational cost by using a coarser grid, i.e. use a 0.4° grid instead of a 0.2°, without decreasing the results' accuracy substantially. Four interpolation functions are tested, i.e. linear, cubic, makima and spline, by comparing the results obtained from these functions with the corresponding results from the 0.2° grid.

2.2. Case-study

The work presented in this study was carried out using a hygrothermal model of a 13th-century church, which was developed in WUFI®Plus [31] and EnergyPlus [37]. In order to develop this model, both the indoor climate and the outdoor climate in the vicinity of the church – temperature and relative humidity – were monitored from November 2011 until August 2013 using a multi-sensor grid with a time frequency of 10 min [42] to comply with the established requirements for this type of monitoring campaign [43].

Whilst the recorded indoor conditions were used to validate the model, the recorded outdoor conditions were used to build the outdoor weather file that the model needs to run proficiently [44]. Aside from the vicinity measured air temperature and relative humidity, the other necessary outdoor parameters were used from a nearby weather station to build a complete outdoor weather file [31].

The church has thick mortared limestone walls (total thickness of 0.9 m [31]), a ceramic tile roof, a limestone slab (total thickness of 0.2 m [31]) and single-glazed windows (U_{window} of 5.1 W/(m^{2}K) [31]), and it is composed by several compartments, namely a nave, a mortuary, and a sacristy, among several other compartments, comprising a total indoor volume of 5250 m^3 (Fig. 1). The church, which is located in the slopes of São Jorge castle in Lisbon, is naturally ventilated and it is not equipped with any type of climate control systems [42].

All these particularities make St. Cristóvão church a representative example of high thermal inertia historic buildings that exist throughout Portugal. Further information about either the monitoring campaign or the computational model can be found elsewhere [31,37,42].

2.3. Map development methodology

The maps shown in this study were developed following the procedure presented in Fig. 2, which is organized in five different blocks. The procedure starts by defining a grid that covers the selected region/country so that the geographical variability of the analysed parameter can be determined (i.e. 229 points in the maps shown in section 3 – Block #1, Fig. 2). The spacing of the grid will greatly affect the accuracy of the shown maps, as well as its computational cost. The finer the grid, the more accurate the developed map, but at the same time the computational cost will be higher, since a greater number of simulations will have to be run. The developed code adapts independently to the selected area/region or to a finer/coarse grid to maximize the use of this

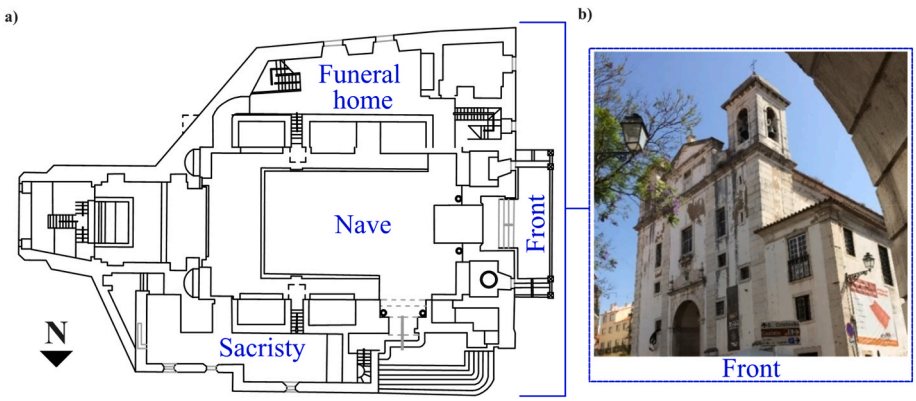

Fig. 1. Plan (a) and picture of the front (b) of St. Cristóvão church [17,42].

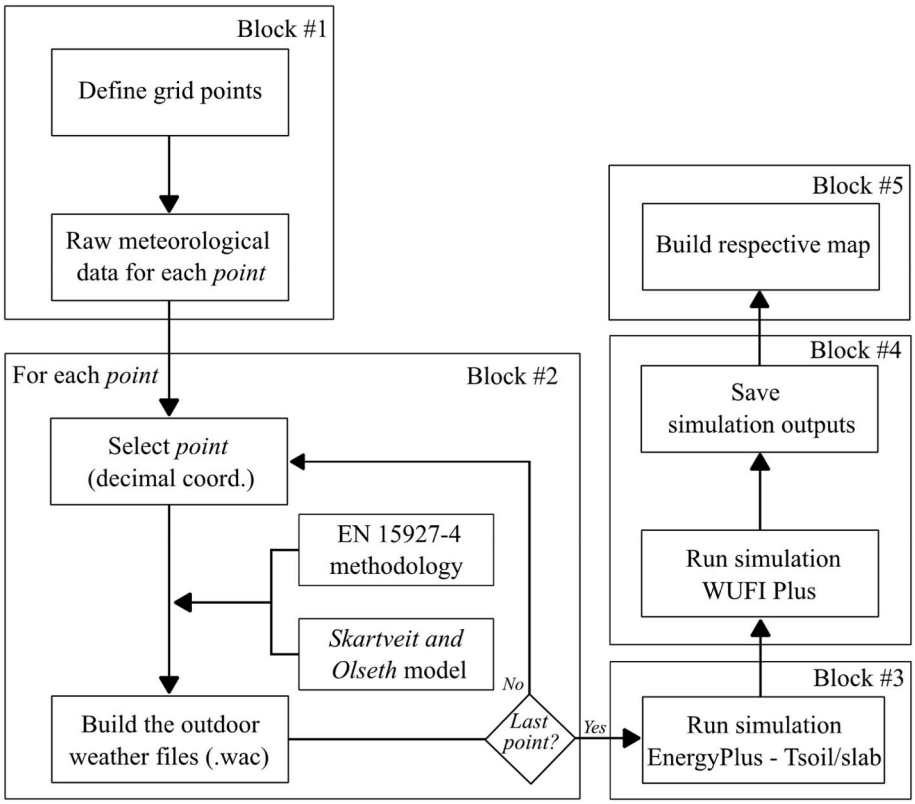

Fig. 2. Methodology to build the variance maps.

methodology.

The meteorological data, which WUFI®Plus needs to run a full hygrothermal simulation [44], was retrieved from the CORDEX files [17] for the previously selected points (Block #1, Fig. 2). The required meteorological data are the following: 1) temperature, 2) relative humidity, 3) air pressure, 4) global radiation and diffuse radiation, 5) atmospheric counter radiation, 6) precipitation, 7) cloud index, 8) wind direction and speed [44]. The CORDEX files are yearly .nc files that cover the whole of Europe and part of North Africa and contain parameter dependent time frequencies. For this study, the used data corresponds to the model HadGEM2-SMHI-RCA4, which accurately simulates the Portuguese climate as shown by two Portuguese research projects [45–47].

Future weather conditions are outputs of complex models that take into account several parameters (e.g. demographic development, socio-economic development, technological evolution and land use change, among others [15]) and their variability through time. Consequently, the evolution of these inputs leads to different possible future conditions. Normally, the predictions' reliability can be assessed by using different model outputs, which are obtained from different models that either have different initial conditions and/or the variability of the parameters that influence the outdoor climate across the period of time is different. Although this is an extremely interesting scientific field, it is the authors belief that it falls outside of the purpose of this study, and it requires the use of very heavy data files that would entail a significant computational effort.

This step is carried out for several periods of time, i.e. near-past (NP), near-future (NF) and far future (FF), as well as for two RCP scenarios, i.e. RCP 4.5 (intermediate scenario) and RCP 8.5 (high GHGs emissions). NP normally corresponds to the thirty-year period at the end of the previous century, 1970 to 1999 in this study. While NF corresponds to mid-21st century, 2020 to 2049 in this study, and FF corresponds to 21st

century end, i.e. 2069 to 2098.

The elevation data was obtained resorting to the European Digital Elevation Model (EU-DEM v1.1) [48], which contains a 25 m spatial resolution with a ca. 7 m RMSE vertical accuracy, and the open source Geographic Information System QGIS [49]. Namely, the sample raster values algorithm, available in QGIS's processing toolbox, was used to extract the raster values (EU-DEM) at the specified point locations.

Secondly, the outdoor weather files were built using the methodology of standard EN 15927-4 [38], with each weather file being built using 30-years' worth of data (Block #2, Fig. 2). This methodology obtains the representative months of the selected locations through a procedure that considers long-term meteorological datasets. The values of temperature, relative humidity and global radiation are used to determine the months with the three-lowest overall rankings. Subsequently, it uses the wind speed for the final selection of the representative month.

The *Skartveit and Olseth* model was used to split the global radiation into its direct and diffuse fractions since WUFI®Plus needs both to perform its simulations [44]. Finally, these weather files were saved in .wac file type [44]. All these operations, which are carried out for the defined grid, are performed by MATLAB so that the process is more time-efficient and less prone to human error [41,50].

Thirdly, the previously built outdoor weather file was automatically introduced in the EnergyPlus model [31] to obtain the soil/slab interface temperature for the selected point (Block #3, Fig. 2). WUFI®Plus needs this input if the simulated model is in direct contact with soil but does not have a model to obtain it. So, one of the EnergyPlus models – the *Detailed ground heat transfer* model [31] – that allows to obtain these values was used, so that the soil/slab interface temperature was both location and period dependent. Fourthly, the previously built outdoor weather file and soil/slab interface temperature were automatically introduced in the model obtained in Block #4. Subsequently, the simulations are run in WUFI®Plus (Block #4, Fig. 2).

After all simulations are carried out, the respective geographical distribution maps are produced (Fig. 3), which allows to analyse the geographical distribution of the selected parameter. This methodology can be applied to several different types of analysis, such as assessing the geographical variance of the indoor climate (e.g. Refs. [9,32]), the artefacts conservation metrics (e.g. Refs. [9,32]), the energy consumption (e.g. Ref. [33]) or even assessing a retrofit potential to mitigate the effects of climate in accordance with the location of the case-study (e.g. like developed by Posani et al. [51], but for wide regions). The inputs and outputs of each of the five steps of the methodology are summarized in Table 1:

In accordance with the time it requires to run each block, either the block was run in a single computer (PC #1 – Intel(R) Core(TM) i5-8500 CPU @ 3.00 GHz and 16 GB of RAM and 64-bit operation system) or in multiple computers (PC #2 – Intel(R) Core(TM) i5-6500 CPU @ 3.20 GHz, 4 GB of RAM and a 64-bit operating system [24]) to compensate for the time it takes to run all the necessary code/simulations to complete the respective block [41].

Table 1
Inputs and outputs for each of the five steps of the developed methodology.

Block	Inputs	Outputs
#1	•Region/country limits •Raw meteorological data	•Grid point location (longitude, latitude & elevation) •Location weather data: 1) temperature, 2) relative humidity, 3) air pressure, 4) global radiation and diffuse radiation, 5) atmospheric counter radiation, 6) precipitation, 7) cloud index, 8) wind direction and speed
#2	•EN 15927-4: 1) temperature, 2) relative humidity, 3) global radiation and 4) Wind speed. Subsequently, the other weather parameters are also used •Skartveit & Olseth: 1) global radiation, 2) extraterrestrial solar radiation, 3) solar elevation	•EN 15927-4: test reference year •Skartveit & Olseth: global radiation spitted in direct and diffuse radiation •Outdoor weather in .wac file format
#3	•Outdoor weather file (.wac) •EnergyPlus model (St. Cristóvão Church [37])	•Soil/slab interface temperature file that is location and period dependent
#4	•Outdoor weather file •Soil/slab interface temperature file •WUFI®Plus model (St. Cristóvão Church [31])	•Indoor conditions - Temperature & Relative humidity for historical values and future conditions
#5	• Indoor conditions	•Built maps

Computer 1 was used for block #1, block #2 and block #3 since these blocks have negligible time consumption when compared to the procedures developed in block #4. To build one map, i.e. using the 229 points that makeup the grid that the authors chose to characterize Portugal: block #1 takes ca. 64 min, block #2 takes ca. 2 min and block #3 takes ca. 48 min. Hence, it takes less than 2 h to perform the first three blocks for the 229 selected locations, i.e. to obtain the necessary inputs – weather file and Tsoil/slab – for one location only takes 30 s.

Multiple instances of the second computer were used for block #4 (takes 209 h to run the 229 sims in PC #1), since it takes a considerable amount of time to run all the necessary hygrothermal simulations [24]. Finally, the maps shown in section 3 were built using PC#1, since it is necessary to gather all the obtained data in one place to build them. The time it takes to build the maps is negligible when compared to the procedures of block #4.

The authors believe that it is essential that this methodology functions independently from the user so that the maps are produced efficiently. For this purpose, an original code was developed in MATLAB that automatically builds these maps integrating all steps shown in Fig. 2. Although this code was originally built for MATLAB it can easily be adapted to other languages, such as, PYTHON.

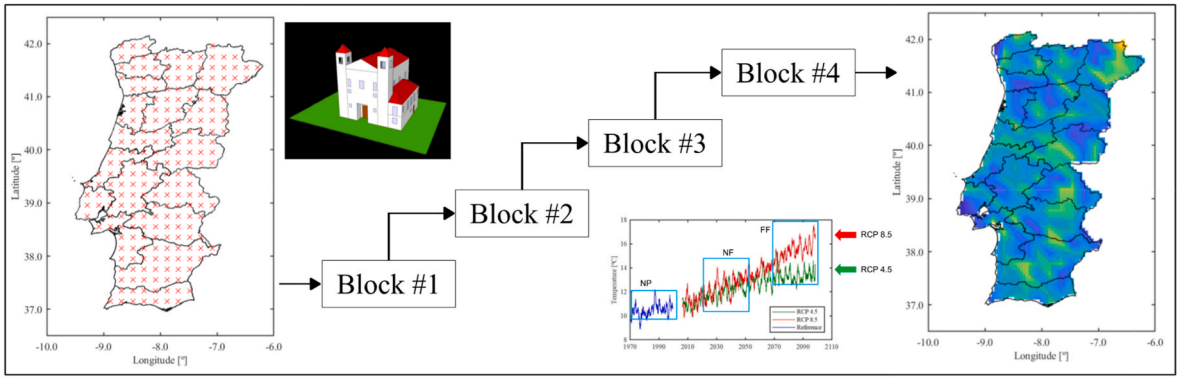

Fig. 3. Overview of the methodology to build the variance maps.

In addition, to verify the accuracy of the developed maps, namely the geographical distribution of annual mean temperature and relative humidity, two grids were generated: 1) a finer grid with a 0.2° spacing (corresponds approximately to 20 km), and 2) a coarser grid with a spacing of 0.4° (corresponds approximately to 40 km). Fig. 4 illustrates the locations used by the finer and coarser grids to determine the indoor conditions and, subsequently, generate the variance maps presented in section 3.3.

Therefore, in order to obtain the variance maps with a 0.2° resolution (constant locations), two paths were followed: 1) the finer grid with a 0.2° spacing was directly used to compute the variance map, and 2) the coarser grid with a 0.4° spacing was employed in combination with several interpolation functions available in MATLAB, i.e. linear, cubic, makima and spline. Note that, to minimize computing time, all locations generated for the coarser grid are also present in the finer grid (see Fig. 4). Moreover, since both grids were used to compute variance maps for the same locations (finer grid), one may readily compare the value attained resorting to both paths. Finally, the computational cost versus the accuracy of each grid was also analysed.

2.4. Portuguese climate

The Köppen classification [52] divides Portugal (continental) in two types of temperate climate [53]: 1) a temperate climate with a rainy winter and a hot and dry Summer (Csa); and 2) a temperate climate with a rainy winter and dry and mild Summer (Csb) [54,55]. Although the climate in Portugal can be generally characterized by being temperate, which is largely influenced by the ocean when dealing with coastal locations, it is also visible that the climate can have significant changes in accordance with the location [54].

For this purpose, six locations with substantial different climates were selected, three coastal locations – Porto, Lisboa and Faro – and three locations in the interior of Portugal – Bragança, Portalegre and Beja, to perform the analysis presented in 3.1 and 3.2. In order to have more accurate assessments, the cities' values presented in 3.1 and 3.2 correspond to the grid point that is nearest to each of the cities' coordinates presented in Table 2.

In terms of the *coastal climates* (Table 2), it is visible that Faro is the warmest climate (highest annual temperature average, 17.4 °C; and lowest heating period, 4.8 months) with the highest annual radiation sum (2040 kWh/m^{2}a), while Porto is the less warm (lowest annual temperature average, 15.8 °C; and highest heating period, 6.2 months) and lowest annual radiation sum (1786 kWh/m^{2}a). On contrast, Porto is the one with the highest annual precipitation (1147 mm/a) and the highest annual relative humidity (81%), while Faro is the one the lowest annual precipitation (509 mm/a) and the lowest annual relative humidity (74%). Finally, Lisbon is the most intermediate climate.

In terms of the *interior climates* (Table 2), it is visible that Beja is the warmest climate although it does not attain the highest temperatures (it has the highest annual average temperature, 17.9 °C, and the lowest heating period, 5 months; but Portalegre attains the highest maximum temperature, 39.0 °C) with Beja having the highest annual radiation sum (2001 kWh/m^{2}a), while Bragança is the less warm (lowest annual temperature average, 13.8 °C; and highest heating period, 7.3 months and attains below zero temperatures) and with a lower annual radiation sum (1731 kWh/m^{2}a). Portalegre has a similar climate to Beja, although normally the values are of lower magnitude. In terms of relative humidity, the three locations have similar values, but in terms of precipitation the highest value corresponds to Portalegre (852 mm/a), followed by Bragança (758 mm/a) and then by Beja (572 mm/a).

Overall, the coastal climates are more moderate climates than the interior climates because of the ocean moderating effect [56]. The values presented in Table 2 were acquired using the *Portuguese reference meteorological years*, which were obtained from LNEG's climate data excel tool [57]. The only exception to this database is the normal rain values, which were taken from the normals for the Portuguese climate developed by The Portuguese Institute for Sea and Atmosphere (IPMA) [58].

3. Results and discussion

This section is divided in three subsections. Firstly, the map-built methodology described previously is used to determine how the indoor air temperature (Figs. 5 and 6) and relative humidity (Figs. 7 and 8) inside high thermal inertia historic buildings are going to be affected by climate change in subsections 3.1 and 3.2, respectively. This assessment is carried out by presenting maps that are built from the difference between a given scenario results – i.e. RCP 4.5 and RCP 8.5 – and time period – i.e. near-future (NF) and far-future (FF) – against the historic values.

This assessment option allows to compare the maps presented in each time period (e.g. Fig. 5a and e) but not between different time

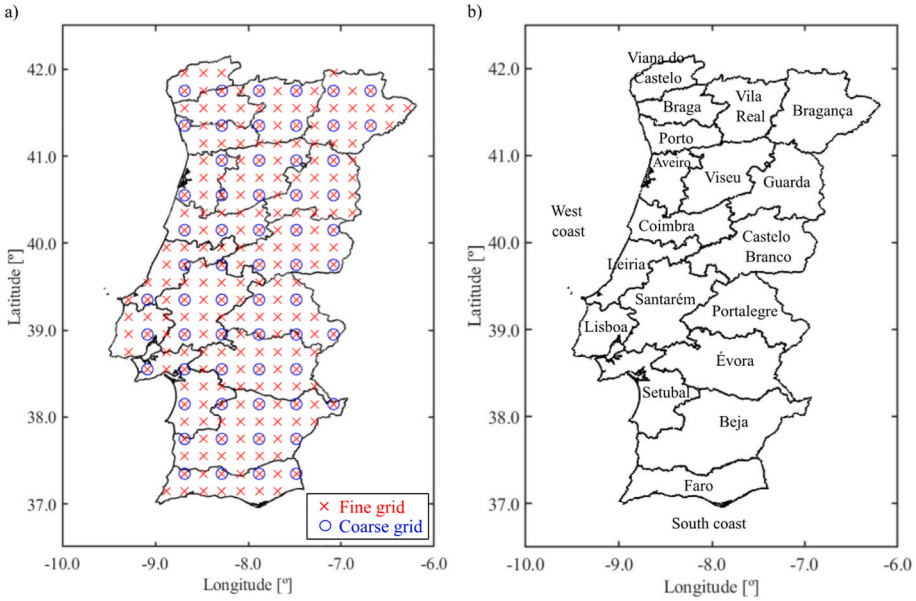

Fig. 4. Fine and coarse grids used in subsections 3.1 & 3.2 and subsection 3.3, respectively (a) and Portugal's districts (b).

Table 2
Overview of the six selected cities climate [57,58] and their respective coordinates.

Climates		Coastal climates			Interior climates		
		Porto	Lisboa	Faro	Bragança	Portalegre	Beja
Temperature (°C)	Max	32.7	32.1	35.0	35.9	39.0	38.5
	Mean	15.8	16.6	17.4	13.8	17.2	17.9
	Min	2.2	3.7	3.3	−2.3	1.4	2.1
Relative humidity (%)	Max	98	98	98	98	99	98
	Mean	81	78	74	75	74	76
	Min	37	32	22	15	15	15
Normal rain (mm/a)		1147	726	509	758	852	572
Radiation horiz. (kWh/m^{2}a)		1786	1938	2040	1731	1920	2001
Heating period (M)		6.2	5.3	4.8	7.3	5.3	5.0
Coordinates	Latitude	41.15°	38.72°	37.02°	41.81°	39.29°	38.02°
	Longitude	−8.61°	−9.13°	−7.93°	−6.76°	−7.43°	−7.86°

periods (e.g. Fig. 5a vs Fig. 6a), since the temperature/relative humidity difference scale differs in accordance with the time period. The *indoor monthly moving average* [59], either air temperature or relative humidity depending on the figure, are also presented in these figures for the highlighted locations. The seasons of the year are also represented in these figures with W corresponding to winter, Sp to spring, S to summer and A to autumn.

Thirdly, the accuracy of the geographical distribution of annual indoor air temperature and relative humidity is assessed resorting to grids with different spacings (0.2° and 0.4° with interpolation) in subsection 3.3. This accuracy is verified both in terms of the absolute difference observed for the annual indoor air temperature (Fig. 9) and the annual relative humidity (Fig. 10). Moreover, the distribution of temperature and relative humidity relative differences according to the used interpolation function is also presented and analysed (Table 3).

3.1. Geographical variance of the indoor air temperature

3.1.1. Near future – RCP 4.5 & RCP 8.5

This subsection addresses the expected variance of the indoor air temperature for high thermal inertia buildings in the near future (NF) in relation to the near past for both assessed RCP scenarios. This variance is shown for RCP 4.5 in Fig. 5a, and for scenario RCP 8.5 in Fig. 5e.

In scenario RCP 4.5, most of the locations have a temperature increase between 0.5 and 1.0 °C, i.e. 96 % of the 229 locations with 2.1% having a higher increase and 1.7% a lower increase (Fig. 5a). While for scenario RCP 8.5, a higher indoor increase is expected (Fig. 5e). Most of the locations have a temperature increase that ranges between 1.0 and 1.5 °C, i.e. 87.8%, with only a small percentage having an increase below this range, i.e. 12.2%. This shows there is a significant shift in terms of indoor temperature for scenario RCP 8.5, which is clearly higher than RCP 4.5.

The difference between the coastal and interior zones is not so evident for scenario RCP 4.5 since most of the country has a similar colour (Fig. 5a). Even so, it is visible that the increase of indoor temperature is slightly lower in the coastal zones than in the interior. For example, if Porto is compared against Bragança (Fig. 5b), it is visible that Porto is a more moderate climate than Bragança since during the cold months the indoor temperature is higher and during the warm months the indoor temperature is lower. Similar trends are visible for the other two sets of assessed climates, but to a lower extent. The big differences between Lisboa and Portalegre occur in the end of spring, the whole summer and the beginning of autumn (Fig. 5c). On the other hand, the big difference between Faro and Beja occurs during the end of winter (Fig. 5d). These differences are logical due to the buffering effect that enormous volumes of water, e.g. oceans and seas, have on moderating the temperature in nearby land [56].

In contrast, for scenario RCP 8.5, a distinction between the west coast and interior zones is much more visible, with the first having an increase of the indoor temperature close to 1.0 °C, whilst for the interior zones, a higher increase is expected that reaches an increase of 1.5 °C (Fig. 5e). This is clearly depicted by the comparison of the indoor temperature variance between Porto and Bragança (Fig. 5f), as well as Lisboa and Portalegre (Fig. 5g), but not so much on the comparison between Faro and Beja (Fig. 5h). Both Portuguese coasts, i.e. west and south, are in contact with the Atlantic Ocean. However, while the Portuguese west coast is characterized by high energetic waves [60], the southern coast is characterized by more moderate wave energy [60], which seems to result in a lower buffering effect.

3.1.2. Far future – RCP 4.5 & RCP 8.5

This subsection presents the expected variance of the indoor air temperature for high thermal inertia buildings in the far future (FF) in relation to the near past. This is shown for scenario RCP 4.5 in Fig. 6a, and then shown for scenario RCP 8.5 in Fig. 6e.

For scenario RCP 4.5, most of the simulated locations have a temperature increase that ranges between 1.5 and 2.0 °C, i.e. 87 % of the 229 locations and 13.1% of these locations have a lower increase (Fig. 6a). Most of the locations indoor temperature increase shifted from the range 0.5–1.0 °C to range 1.5–2.0 °C from the near to the far-future for this scenario, which shows the general expected trend in terms of indoor temperature. For scenario RCP 8.5, most simulated locations, i.e. 58 %, have a temperature increase that ranges between 2.5 and 3.0 °C, and 29.7% of the locations have even a higher increase. These quite significant shifts clearly show that RCP 8.5 in the far future is the most affecting scenario, which is understandable while considering what was mentioned in section 1.

The difference between the coastal and interior zones is not so evident for scenario RCP 4.5. However, it is visible that the increase of the indoor temperature is slightly lower in the coastal zones (lighter yellow, which corresponds to a lower temperature increase, Fig. 6a) than in the interior zones (darker yellow, which corresponds to a higher temperature increase, Fig. 6a). In contrast, for scenario RCP 8.5, a distinction between the west coast and the interior zones is much more visible, when compared with RCP 4.5 (Fig. 6a and e). In addition, and differently from the near-future (Fig. 5), it is also visible a clear distinction between the south coast and the interior zones.

By comparing Porto and Bragança for scenario RCP 4.5, it is visible that the increases are similar throughout the year with the more significant differences occurring in winter, and during the last part of the summer and the beginning-mid autumn, the difference is a rather constant, i.e. 0.6 °C (Fig. 6b). It is evident that Porto still has a more temperate climate than Bragança. For Lisbon and Portalegre, the major differences occur during summer, and at a lower extent during the beginning of autumn, since for the remaining of the year, the two increases are similar (Fig. 6c). Lisbon still has a more moderate climate than Portalegre, specially during warmer months (Fig. 6c). The major difference for Faro and Beja seems to occur in winter, and at the border between spring and summer (Fig. 6d).

On the other hand, for scenario RCP 8.5, significant differences exist

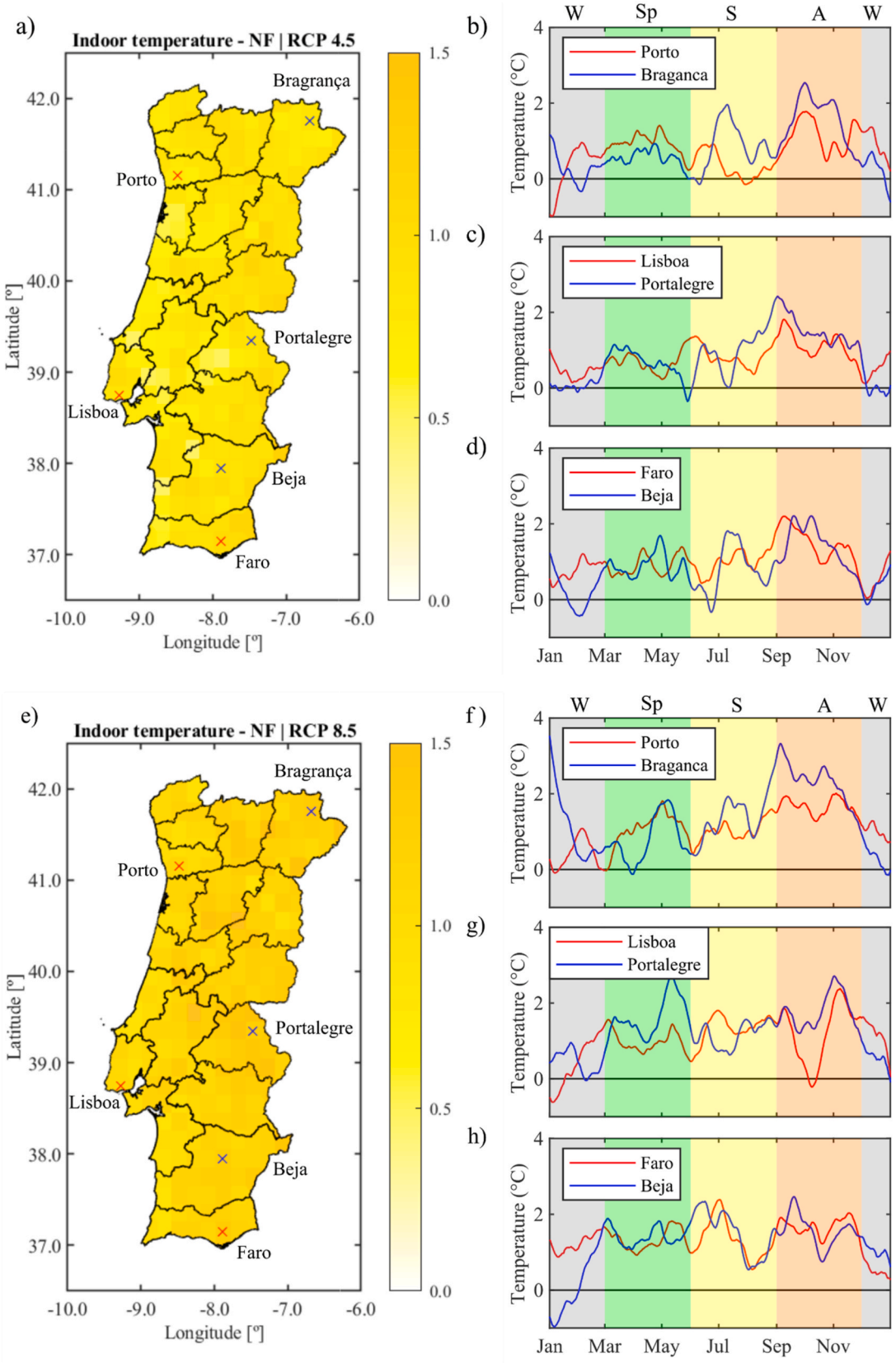

Fig. 5. Geographical distribution of the *annual mean indoor air temperature* for **RCP 4.5** in the near-future (NF) climate minus the reference climate for Portugal (a) and indoor monthly moving average for Porto vs Bragrança (b), Lisboa vs Portalegre (c) and Faro vs Beja (d); and Geographical distribution of the *annual mean indoor air temperature* for **RCP 8.5** in the near future (NF) climate minus the reference climate for Portugal (e) and indoor monthly moving average for Porto vs Bragrança (f), Lisboa vs Portalegre (g) and Faro vs Beja (h).

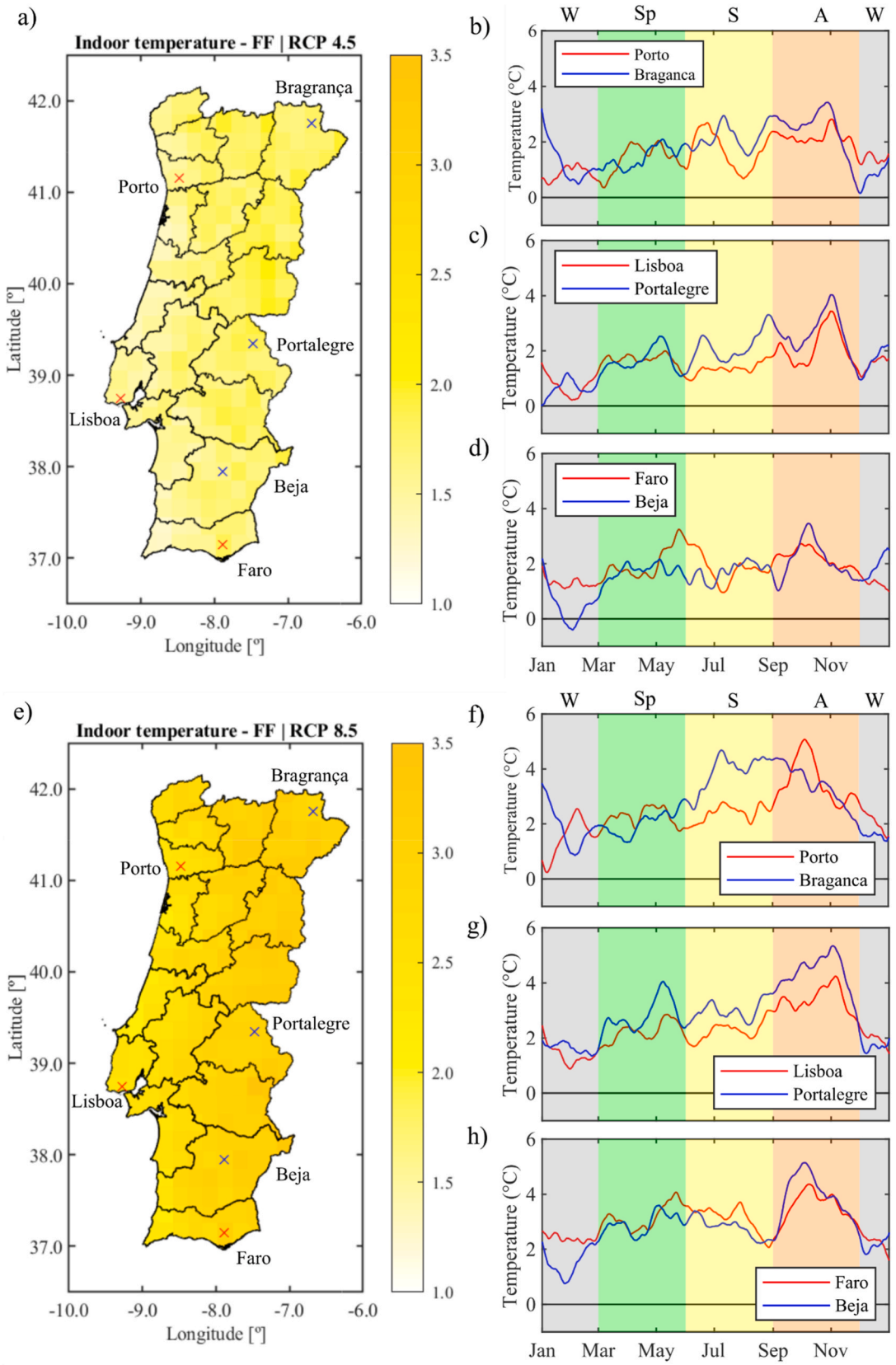

Fig. 6. Geographical distribution of the *annual mean indoor air temperature* for **RCP 4.5** in the far future (FF) climate minus the reference climate for Portugal (a) and indoor monthly moving average for Porto vs Bragrança (b), Lisboa vs Portalegre (c) and Faro vs Beja (d); and Geographical distribution of the *annual mean indoor air temperature* for **RCP 8.5** in the far future (FF) climate minus the reference climate for Portugal (e) and indoor monthly moving average for Porto vs Bragrança (f), Lisboa vs Portalegre (g) and Faro vs Beja (h).

between Porto and Bragança throughout the year, but they are more substantial during the summer (Fig. 6f). In addition, it is visible that Porto has a much more temperate climate than Bragança (Fig. 6f). A major constant difference between Lisboa and Portalegre is observed during the whole summer, and the whole autumn, as well during some periods in spring (Fig. 6g). Once again, it is visible that the coastal climate has a more temperate climate than the interior climate, especially in the warm months (Fig. 6g). Finally, no substantial distinction between Faro and Beja is observed, except at the end of winter, and at the beginning of autumn (Fig. 6h).

3.2. Geographical variance of the indoor air relative humidity

3.2.1. Near future – RCP 4.5 & RCP 8.5

This subsection presents the expected geographical variance of the indoor relative humidity in the near future in relation to the near past. This analysis is firstly shown for RCP 4.5 (Fig. 7a) and then for RCP 8.5 (Fig. 7e). The analysis of the indoor temperature can be assumed to be much more reliable than the analysis of the relative humidity, due to the substantial variability nature of RH, which is both moisture and temperature dependent. For example, when T increases, RH decreases, but on the other hand, when moisture increases, RH increases [61]. Nonetheless, it is quite interesting to assess the RH for this kind of buildings due to its great influence on the conservation of artefacts [2].

It is visible that for the majority of the coastal zones – west and south – an increase of relative humidity is expected for scenario RCP 4.5 (Fig. 7a), whilst in some interior regions, i.e. Portalegre and Beja districts, a decrease of the relative humidity is expected in the near future. This behaviour is noticeable by comparing, for example, Lisboa and Portalegre as well as Faro and Beja, i.e. a coastal location versus an interior location. In conclusion, most of the simulated locations have a relative humidity increase of 0.0–3.0%, i.e. 84 %, with 6.6% having a higher increase and 14.4% of the locations corresponding to a decrease of indoor RH.

Generally, a similar behaviour for scenario RCP 8.5 is observed when compared with RCP 4.5 (Fig. 7a and e), i.e. in the majority of the coastal zones, an increase of relative humidity is expected, whilst in some zones of the eastern interior regions of Portugal (i.e. Beja, Évora and Portalegre), a decrease of the relative humidity is expected in the near future. By comparing the results for RCP 4.5 and 8.5 is possible to observe singular differences, e.g. in Bragança the increase is higher (1.3% for RCP 4.5 and 3.1% for RCP 8.5), but Portalegre changes from a decrease of RH of -0.5% for RCP 4.5 to an increase of 0.6% for RCP 8.5. For scenario RCP 8.5, most of the locations have a relative humidity increase of 0.0–3.0%, i.e. 90 %, with 1.7% having a higher increase and 7.9% corresponding to a decrease.

For the six selected locations, different behaviours are observed. An increase of the indoor relative humidity is expected for Porto and Bragança (Fig. 7a), but to a higher extent for Porto (2.3%) than for Bragança (1.3%). On contrary, opposite behaviours are seen for Lisboa and Portelegre. While the indoor RH in Lisboa is expected to increase (1.6%), it will decrease for Portalegre (-0.5%) in comparison with the near past (Fig. 7a). The major differences occur at the end of summer, and during most of autumn. Finally, opposite behaviours are also seen for Faro and Beja. While the indoor RH in Faro is expected to slightly increase (0.4%), it is expected to decrease for Beja (-0.9%) (Fig. 7a). The major differences between them occur during the spring and summer.

An increase of the indoor RH is expected for both Porto and Bragança if the world evolves as described by RCP 8.5 in the near future (Fig. 7e), but to higher extent for Bragança (3.1%) than for Porto (2.5%). In fact, these locations have a similar trend throughout the year (Fig. 7f) with the exceptions occurring mostly in spring, and in summer. The expected indoor RH increase is similar for Lisboa and Portalegre (Fig. 7e), i.e. 1.4% and 0.6%, respectively. In fact, the evolution of the RH trend for these two locations is quite similar (Fig. 7g), with the major differences occurring during the end of spring, though there are other smaller differences that occur during the other seasons, e.g. the peaks detected in summer (Fig. 7g). Finally, the opposite behaviour is observed in Faro and Beja (Fig. 7e). While in Faro an increase of the indoor RH of 2.5% is expected, a decrease of -0.5% is expected for Beja. This is clearly seen in the monthly mean moving average comparison between these two locations (Fig. 7h).

3.2.2. Far future – RCP 4.5 & RCP 8.5

Here, it is shown the expected variance of the relative humidity of the indoor air in the far future in relation to the near past, firstly for RCP 4.5 (Fig. 8a) and then for RCP 8.5 (Fig. 8e).

An increase of relative humidity is expected in both coastal zones of Portugal, although the magnitude of these increase varies for scenario RCP 4.5 (Fig. 8a). In the east interior regions of Portalegre, Évora and Beja districts, a decrease of the relative humidity is expected in the far future, while it is also visible for some zones of the districts of Castelo Branco and Faro but limited to smaller areas when compared to the first three mentioned districts. These different behaviours are visible, e.g comparing Lisboa and Portalegre. Most of the locations have a relative humidity increase of 0.0–3.0%, i.e. 79.4%, with 12.7% having a higher increase and 7.9% corresponding to a decrease.

Conversely, an increase of relative humidity is expected for both coastal zones for scenario RCP 8.5, but much more significant for the west coast when compared with scenario RCP 4.5 (Fig. 8a and e). Whilst in the east interior regions of Évora and Beja districts and somehow Portalegre, a decrease of the relative humidity is expected. However, these decreases occur in a smaller area when compared with the RCP 4.5 (Fig. 8a and e). These different behaviours are visible comparing, e.g. Faro and Beja. Most of the assessed locations have a relative humidity increase of 0.0–3.0%, i.e. 65.5%, with 28.8% having a higher increase and 5.7% corresponding to a decrease.

Different behaviours are observed in the six selected locations for scenario RCP 4.5. An increase of the indoor relative humidity is expected for Porto and Bragança (Fig. 8a), but to a higher extent for the first climate, i.e. 2.6 and 1.3%, respectively. The major differences between these locations occur during summer and the end of autumn. On the other hand, Lisboa and Portelegre are expected to behave with opposite trends (Fig. 8a). The indoor RH in Lisboa is expected to increase by 3.2% and to decrease by -0.6% for Portalegre. The major difference between them occurs during the second half of the spring, at the end of summer, and during the first half of autumn (Fig. 8c). Lastly, similar behaviours for most of the year are observed for Faro and Beja (Fig. 8d). The indoor RH in Faro is expected to increase by 1.5%, closely followed by Beja's, i.e. 1.0%. The major differences are visible during spring, but they are also visible, to a lower extent, during summer (Fig. 8d).

All the six selected climates have similar behaviour, at different extents, for scenario RCP 8.5, i.e. increase of the indoor relative humidity. An increase of the indoor relative humidity is expected for Porto and Bragrança (Fig. 8e), but to a higher extent for the first, i.e. 3.9 and 2.7%, respectively. The major differences are visible during the summer, and the end of autumn (Fig. 8f). Secondly, Lisboa and Portelegre are expected to have similar behaviours, since they have a very similar trend for most of the year (Fig. 8g), with increases of 2.6% and 1.2%, respectively. The major differences are visible during the second half of summer, and at the second half of autumn. Lastly, Faro and Beja have similar behaviours but to very different extents, i.e. increases of 2.7% and 0.5%, respectively (Fig. 8e). The major differences are visible during spring, but also in the end of the summer (Fig. 8h).

3.3. Geographical finesse grid influence on the results

The present section reports the study conducted to verify the accuracy of the geographical distribution of the historical annual indoor air temperature and relative humidity. The accuracy was verified by means of the difference between the results determined on a 0.2° spacing grid resorting to two grids with distinct spacings. Namely, a 0.2° spacing grid

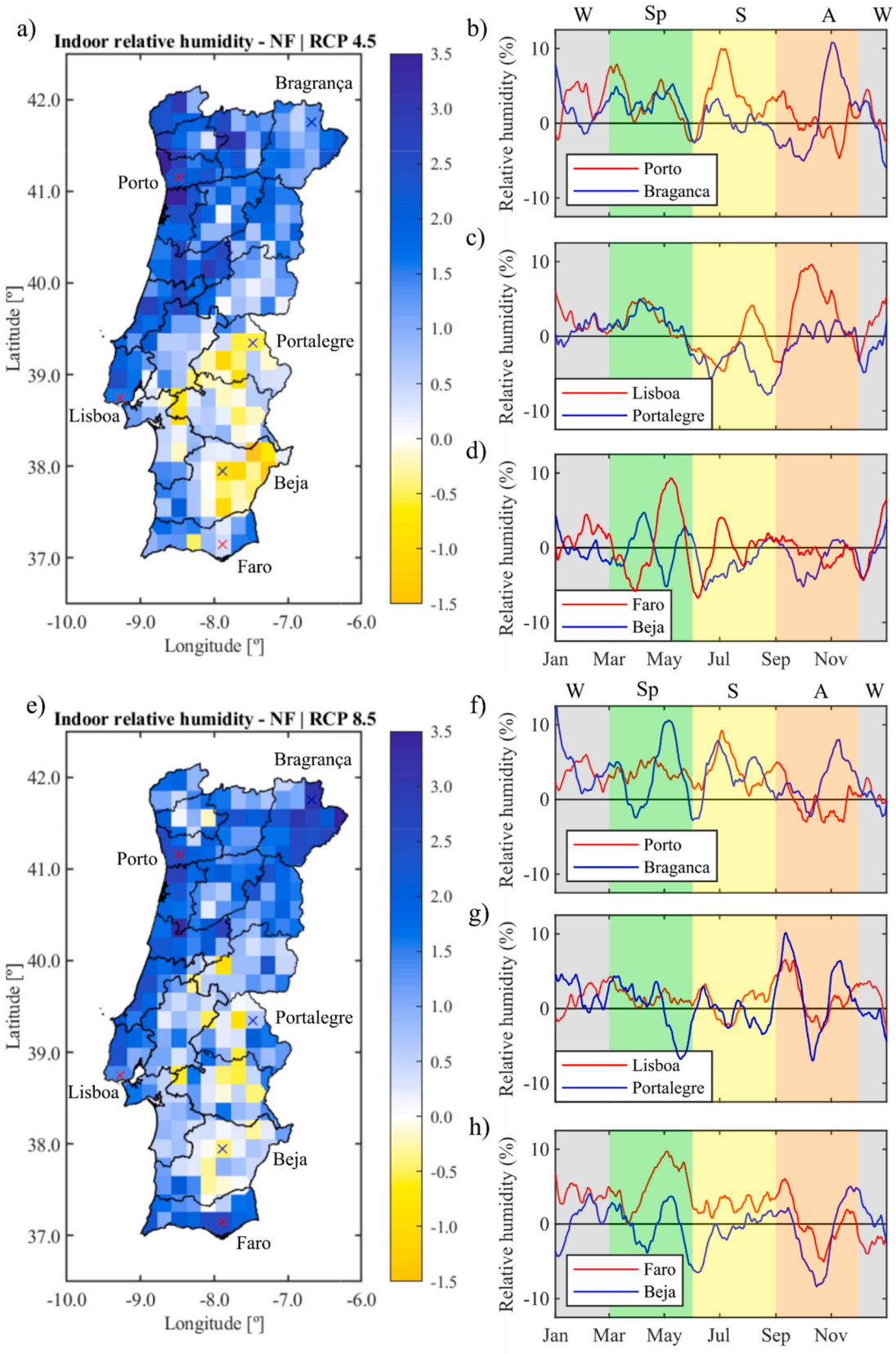

Fig. 7. Geographical distribution of the *annual mean indoor relative humidity* for **RCP 4.5** in the near future (NF) climate minus the reference climate for Portugal (a) and the indoor monthly moving average for Porto vs Bragrança (b), Lisboa vs Portalegre (c) and Faro vs Beja (d); and Geographical distribution of the *annual mean indoor relative humidity* for **RCP 8.5** in the near future (NF) climate minus the reference climate for Portugal (e) and the indoor monthly moving average for Porto vs Bragrança (f), Lisboa vs Portalegre (g) and Faro vs Beja (h).

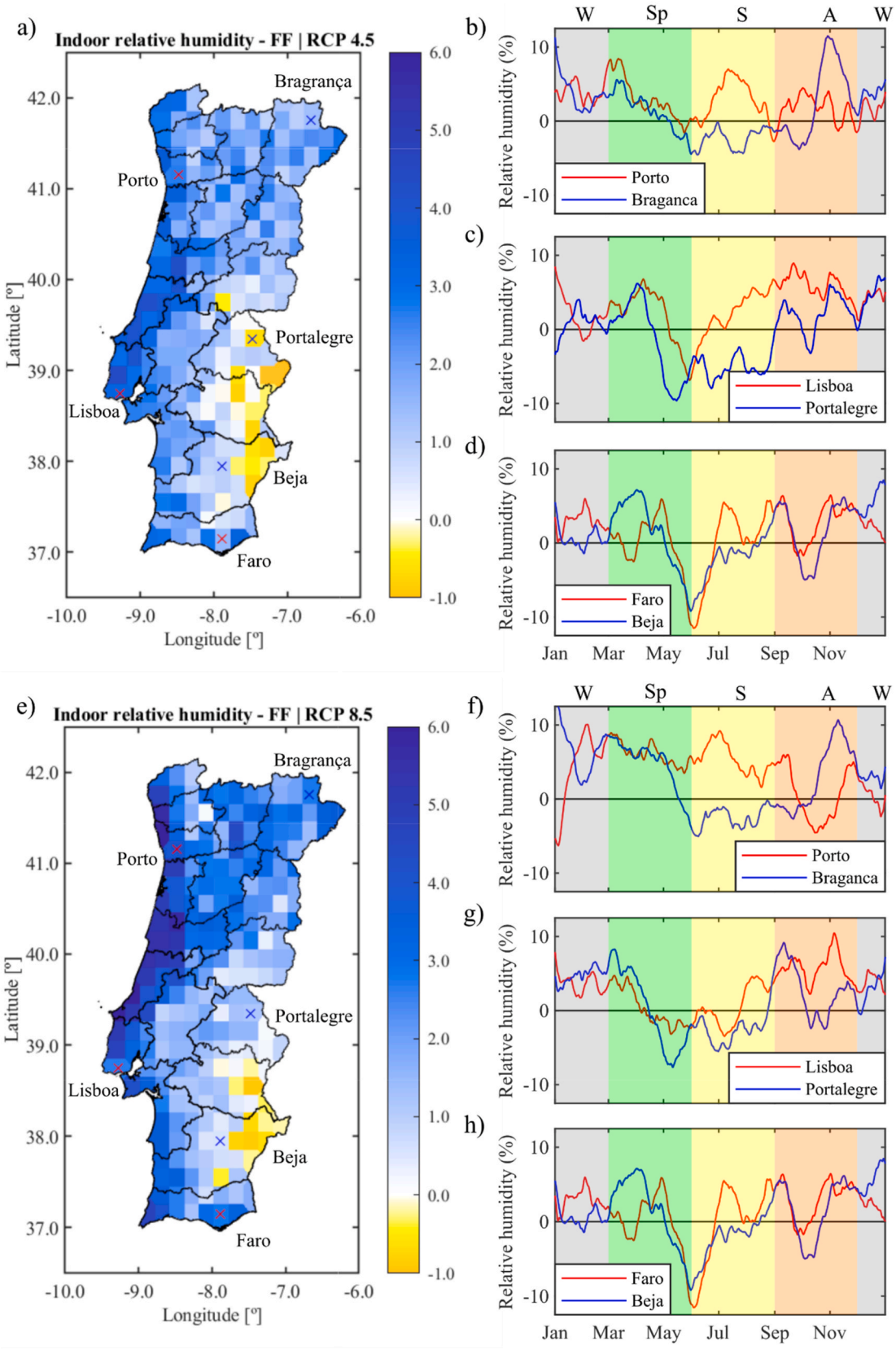

Fig. 8. Geographical distribution of the *annual mean indoor relative humidity* for **RCP 4.5** in the far future (FF) climate minus the reference climate for Portugal (a) and the indoor monthly moving average for Porto vs Bragrança (b), Lisboa vs Portalegre (c), and Faro vs Beja (d); and Geographical distribution of the *annual mean indoor relative humidity* for **RCP 8.5** in the far future (FF) climate minus the reference climate for Portugal (e) and the indoor monthly moving average for Porto vs Bragrança (f), Lisboa vs Portalegre (g), and Faro vs Beja (h).

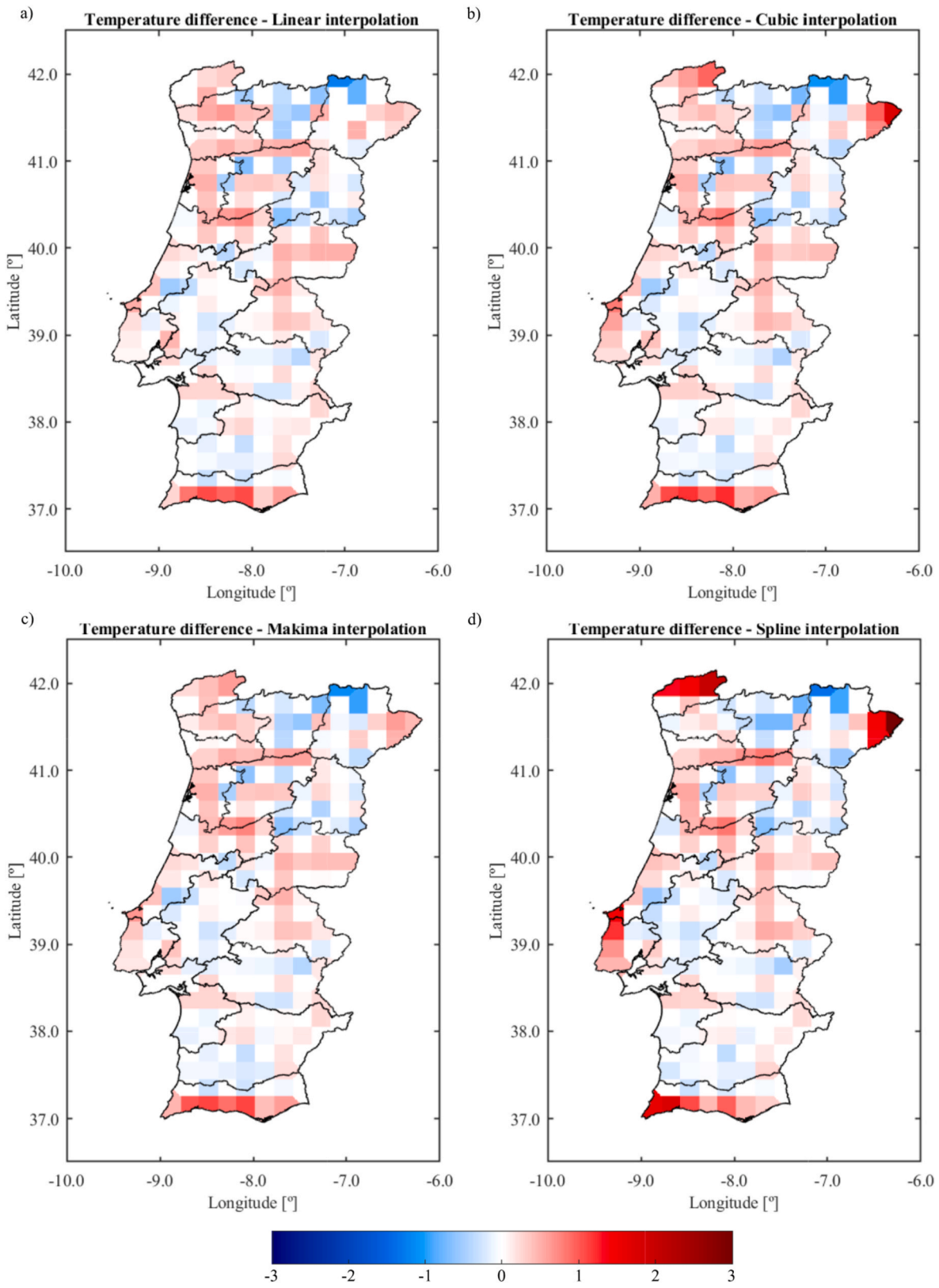

Fig. 9. Geographical distribution in Portugal for the difference in **annual mean indoor air temperature**: 0.2° spacing grid minus the 0.4° spacing grid with a Linear interpolation (a), a Cubic interpolation (b), a Makima interpolation (c) and a Spline interpolation.

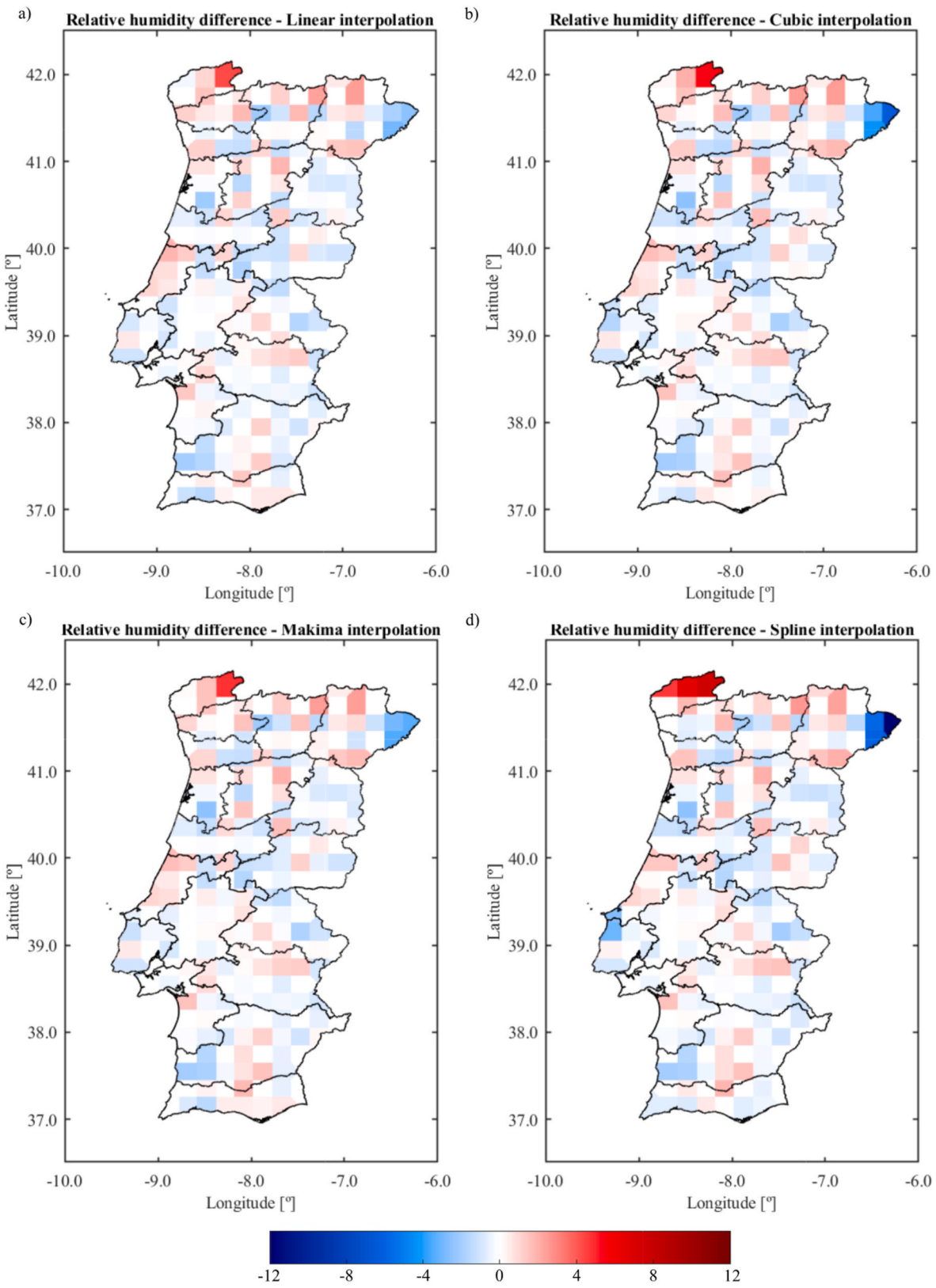

Fig. 10. Geographical distribution in Portugal for the difference in **annual mean indoor air relative humidity**: 0.2° spacing grid minus the 0.4° spacing grid with a Linear interpolation (a), a Cubic interpolation (b), a Makima interpolation (c) and a Spline interpolation.

Table 3
Distribution of the **annual mean indoor air temperature**'s differences and the **annual mean indoor relative humidity**'s differences according to the used interpolation function.

Interpolation function	Temperature [°C]					Relative humidity [%]				
	Average	Percentile		Adjacent values		Average	Percentile		Adjacent values	
		25th	75th	Lower	Upper		25th	75th	Lower	Upper
Linear	−0.09	−0.30	0.11	−0.86	0.67	0.11	−0.55	0.84	−2.37	2.52
Cubic	−0.11	−0.32	0.12	−0.97	0.73	0.12	−0.57	0.86	−2.48	2.41
Makima	−0.09	−0.32	0.12	−0.89	0.69	0.09	−0.55	0.76	−2.44	2.42
Spline	−0.15	−0.31	0.14	−0.97	0.80	0.14	−0.69	0.81	−2.60	2.67

(approximately 20 km), which was used throughout the whole mapping methodology (in subsections 3.1 and 3.2) and a coarser grid (i.e. a 0.4° spacing, which corresponds to approximately 40 km) used in combination with an interpolation function. An analysis is conducted to obtain the differences in terms of annual mean indoor air temperature and relative humidity according to the used interpolation function and verify the influence of the interpolation's smoothing effect on the attained geographical distribution.

The difference in terms of annual mean indoor air temperature and relative humidity, respectively, between the coarser and finer grid (coarse minus fine) according to the used interpolation function are illustrated in Figs. 9 and 10. A positive difference indicates that the interpolation function computes a larger value when compared with the finer grid, whilst a negative difference implies an underestimation of the correct value. As expected, null differences are obtained at the locations shared by both grids, regardless of the considered interpolation function, since no interpolation is required.

Through the analysis of these figures, it is possible to verify that, at locations where the interpolation function does not require extrapolation, smaller differences are observed when compared with locations at which extrapolation is necessary. These larger differences are especially noticeable for the cubic and spline interpolations. Specifically, when the linear and makima interpolation functions are used for extrapolation, absolute differences between -5 and 5% relative humidity are attained, while the cubic and spline interpolation functions yield absolute differences in terms of relative humidity raging between -7.5 and 12%.

The average, 25th and 75th percentiles and the most extreme data point that is not an outlier, henceforth referred to as *adjacent values*, of the annual mean indoor air temperature and relative humidity are summarized in Table 3, depending on the used interpolation function. Analysing the referred table, one may verify that all interpolation functions yield average values close to zero in terms of annual mean indoor air temperature's difference, with the linear and makima interpolations function resulting in the lowest average difference (i.e. -0.09 °C).

Additionally, the linear interpolation has the upper and lower adjacent values closest to zero and, consequently, the smallest standard deviation. Alternatively, the cubic and spline interpolation functions yield the largest standard deviations due to the large differences observed at locations where extrapolation is required.

In terms of the annual mean indoor relative humidity's differences presented in Table 3, the depicted average values are also very close to null, with the largest absolute difference taking a value of 0.14% relative humidity. When comparing the upper and lower adjacent values attained by the several interpolation functions, one verifies that the linear and the cubic lead to the lower and upper adjacent values closest to zero, respectively. The linear interpolation function yields the smallest standard deviation. Additionally, when analysing the computed differences for the near and far future geographical distributions of annual mean indoor temperature and relative humidity, similar conclusions were attained.

If one only considers the differences summarized in Table 3, all interpolation functions yield low differences on average and may be considered as adequate. However, through the observation of the geographic distributions illustrated in Figs. 9 and 10, it possible to verify some interpolation functions greatly over and under predict the finer grid values at locations where extrapolation is necessary, highlighting the importance of analysing the geographic distribution.

The computational cost versus accuracy of each grid was also analysed. Therefore, resorting to the time required to perform the complete mapping procedure for one point (approximately 55 min), one may verify that the coarser grid, which contains 60 locations, requires 55 h to determine the geographical distribution of the annual mean temperature and relative humidity in Portugal. This corresponds to 26% of the time spent to generate the geographical variance of the indoor conditions presented in subsections 3.1 and 3.2, which were determined resorting to the 0.2° spacing grid. Nonetheless, when comparing the results obtained resorting to the finer grid and coarser grid together with the linear or makima interpolation function, maximum relative differences between approximately -10 and 7% are observed for the annual mean temperature, while the annual mean relative humidity's relative differences range between approximately -6 and 7.5%. Moreover, the 5th and 95th percentile do not surpass ±4% for temperature (±1 °C) and ±3% for relative humidity (±3 %RH), clearly indicating that the coarser grid is advantageous, since a 74% decrease in required time is achieved with relatively low errors.

Alternatively, if a finer grid is required, the 0.2° spacing grid may be used in combination with the linear or makima interpolation functions to obtain the annual mean temperature and relative humidity with a finer spatial resolution, since the meteorological data used in the present study is available for a 0.2° spacing grid.

4. Conclusions

This paper studies the geographical variance of the indoor climate of historic buildings of high thermal inertia under current and future conditions to determine how these conditions are expected to evolve due to climate change. This effort will enable to determine the areas in Portugal more susceptible to the effects of climate change, and, therefore, implement proper changes fitted for each location to safeguard the indoor climate.

For this purpose, a five-step methodology was developed by means of using several different tools – e.g. building's computational models, future and historic weather files, among others – connected through MATLAB. The methodology is flexible in whole its five major components and it is user independent, which is excellent since it decreases user error associated to monotonous activities. In order to build one map – i.e. 229 locations – each of the first four blocks, which compose the developed methodology, took the following time:

- Block #1 (*Set the meteorological data*, method #1) – took ca. 64 min;
- Block #2 (*Build the outdoor weather file*, method #1) – tool ca. 2 min;
- Block #3 (*Obtain Tsoil/slab*, method #1) – took ca. 48 min;
- Block #4 (*Obtain Simulation outputs*, method #2) – took ca. 209 h.

It took less than 2 h to perform the first three blocks for the 229 selected locations. Hence, it took less than 2 h to obtain the necessary inputs to run the hygrothermal simulation in block #4, i.e. the outdoor

weather files and Tsoil/slab files. This means that it took only 30 s to obtain these inputs for each location. It is also visible that block #4 is the most time demanding, but this can be lessened by using more powerful computers than the ones that were used in this study or even use a larger amount of computers. On the other hand, the time it took to perform block #5 is negligible compared to most of the other blocks – i.e. took less than 7 s to build each map.

The developed methodology to show data in accordance with location (i.e. maps) is independent from the used computational model. This means that it can easily adapted to other models or even use more than one model at time. This latter option allows, if necessary, to use a representative building in accordance with each region of Europe. Additionally, this methodology can be fitted to any region or country or even use a finer or a coarser grid depending on the aims of the carried-out study. An improvement to the grid's definition block of the methodology is envision by producing more grid points outside the limits of the region that is being analysed when it is a land bordering region (e.g. Bragança border with the respective Spain region) or include grid points at the region limits when it is a water bordering region (e.g. coastal area of the Lisbon region with the Atlantic ocean). In total, 1145 hygrothermal simulations were run to build the therein presented maps.

In terms of the assessment of the indoor conditions, it was seen that the buffering effect that the ocean has on the coastal area is transmitted to their respective indoor climates. It was also seen that the coastal indoor climates are more moderate than the interior ones, although the buffering effect is higher in the west coast than in the south coast. Note that the results presented here were obtained using a calibrated hygrothermal model of a high thermal inertia historic building. This has to be taken into account in case its results and conclusions are to be used for other cases, especially for non-high thermal inertia historic buildings.

It was also shown that there is a significant increase in terms of indoor temperature from scenario RCP 4.5, 96% of the locations have an increase of 0.5–1.0 °C, to scenario RCP 8.5, 88% of the locations have increases of 1.0–1.5 °C, in the near future. This behaviour has even a bigger magnitude in the far future, i.e. 87 % of the locations have an increase of 1.5–2.0 °C for RCP 4.5 and 58% of the locations have an increase of 2.5–3.0 °C for RCP 8.5.

In terms of relative humidity in the near future, it was shown that in the majority of the coastal zones, an increase is expected, whilst in some interior regions, i.e. more significantly for Beja, Évora and Portalegre districts, a decrease is expected, which will gradually lose importance as time advances. For RCP 4.5 in the near future, 84% of the simulated locations are expected to have an increase of the indoor RH of 0.0–3.0%, while the same concept rises to 90% for RCP 8.5. In the far future, a greater number of locations will have a higher increase than 3.0%, i.e. 12.7% for RCP 4.5 and 28.8% for RCP 8.5, while these percentages were respectively only 6.6% and 1.7% in the near future. This shows that gradually, most of the country, is expected to have an increase of indoor RH.

Finally, the accuracy of the geographical distribution of the annual indoor air temperature and relative humidity determined for a 0.2° spacing grid was verified in the present study. Through the comparison of the results determined resorting to the 0.2° spacing grid and to a grid with a 0.4° spacing in combination with several interpolation functions, one may conclude that, when an adequate interpolation function was used, the coarser grid was able to correctly simulate the geographical distribution of annual indoor air temperature and relative humidity. At the locations in which extrapolation was not performed, small differences were achieved, whilst some interpolation functions greatly over and under predict the finer grid value at locations where extrapolation was necessary. Moreover, a 74% decrease in required time was achieved with relatively low errors (±4% for temperature and ±3% for relative) when the linear or makima interpolation functions were used.

CRediT authorship contribution statement

Guilherme B.A. Coelho: Writing – original draft, Visualization, Validation, Software, Methodology, Investigation, Formal analysis, Conceptualization. **Hugo B. Rebelo:** Writing – original draft, Visualization, Validation, Software, Methodology, Investigation, Formal analysis. **Vasco Peixoto De Freitas:** Writing – review & editing, Validation, Methodology, Conceptualization. **Fernando M.A. Henriques:** Writing – review & editing, Validation, Methodology, Conceptualization. **Lourenço Sousa:** Investigation.

Declaration of competing interest

The authors declare that they have no known competing financial interests or personal relationships that could have appeared to influence the work reported in this paper.

Data availability

Data will be made available on request.

Acknowledgments

The first author acknowledges the FCT – *Fundação para Ciência e a Tecnologia* – for the financial support through the PhD scholarship PD/BD/127844/2016. The second author is grateful for the FCT support through funding UIDB/04625/2020 from the research unit CERIS. The third author acknowledges the financially support by UID/ECI/04708/2019 CONSTRUCT – Instituto de I&D em Estruturas e Construções funded by national funds through the FCT/MCTES (PIDDAC).

References

[1] D. Camuffo, Microclimate for Cultural Heritage: Conservation, Restoration, and Maintenance of Indoor and Outdoor Monuments, second ed., Elsevier Science, 2014.
[2] M. Martens, Climate Risk Assessment in Museums: Degradation Risks Determined from Temperature and Relative Humidity Data (PhD Thesis), Technische Universiteit Eindhoven, Eindhoven, 2012, https://doi.org/10.6100/IR729797.
[3] G. Grottesi, G.B.A. Coelho, D. Kraniotis, Heat and moisture induced stress and strain in wooden artefacts and elements in heritage buildings: a review, Appl. Sci. 13 (2023) 7251, https://doi.org/10.3390/app13127251.
[4] R.P. Kramer, J. van Schijndel, H. Schellen, Dynamic setpoint control for museum indoor climate conditioning integrating collection and comfort requirements: development and energy impact for Europe, Build. Environ. 118 (2017) 14–31, https://doi.org/10.1016/j.buildenv.2017.03.028.
[5] P.O. Fanger, Thermal Comfort. Analysis and Applications in Environmental Engineering, Danish Technical Press, Copenhagen, Denmark, 1970.
[6] R. de Dear, G.S. Brager, D. Cooper, Developing an Adaptive Model of Thermal Comfort and Preference - Final Report on RP-884, 1997.
[7] C. Ornelas, J.M. Guedes, I. Breda-Vázquez, Cultural built heritage and intervention criteria: a systematic analysis of building codes and legislation of Southern European countries, J. Cult. Herit. 20 (2016) 725–732, https://doi.org/10.1016/j.culher.2016.02.013.
[8] M. Posani, R. Veiga, V.P. de Freitas, Retrofitting historic walls: feasibility of thermal insulation and suitability of thermal mortars, Heritage 4 (2021) 2009–2022, https://doi.org/10.3390/HERITAGE4030114.
[9] Z. Huijbregts, M.H.J. Martens, C.M.H. Conen, I.M. Nugteren, A.W.M. van Schijndel, H.L. Schellen, Damage risk assessment of museum objects in historic buildings due to shifting climate zones in Europe, in: Proceedings of the 5th International Building Physics Conference, Kyoto, 2012, pp. 1271–1278, 28-31 May 2012.
[10] F. Roberti, U.F. Oberegger, A. Gasparella, Calibrating historic building energy models to hourly indoor air and surface temperatures: methodology and case study, Energy Build. 108 (2015) 236–243, https://doi.org/10.1016/j.enbuild.2015.09.010.
[11] N. Aste, R.S. Adhikari, M. Buzzetti, S. Della Torre, C. Del Pero, H.e.H.C. F. Leonforte, Microclimatic monitoring of the Duomo (Milan Cathedral): risks-based analysis for the conservation of its cultural heritage, Build. Environ. 148 (2019) 240–257. S0360132318307108.
[12] H.E. Huerto-Cardenas, N. Aste, C. Del Pero, S. Della Torre, F. Leonforte, Effects of climate change on the future of heritage buildings: case study and applied methodology, Climate 9 (2021) 132, https://doi.org/10.3390/cli9080132.
[13] F. Antretter, T. Schöpfer, R. Kilian, An approach to assess future climate change effects on indoor climate of a historic stone church, in: 9th Nordic Symposium on Building Physics, 2011.

[14] P. Choidis, G.B.A. Coelho, D. Kraniotis, Assessment of frost damage risk in a historic masonry wall due to climate change, Adv. Geosci. 58 (2023) 157–175, https://doi.org/10.5194/adgeo-58-157-2023.

[15] N. Nakicenovic, J. Alcamo, G. Davis, B. de Vries, J. Fenhann, S. Gaffin, K. Gregory, A. Griibler, T.Y. Jung, T. Kram, E.L. La Rovere, L. Michaelis, S. Mori, T. Morita, W. Pepper, H. Pitcher, L. Price, K. Riahi, A. Roehrl, H.-H. Rogner, A. Sankovski, M. Schlesinger, P. Shukla, S. Smith, R. Swart, S. van Rooijen, N. Victor, Z. Dadi, Special Report on Emissions Scenarios - A Special Report of Working Group III of the Intergovernmental Panel on Climate Change, Cambridge University Press, 2000.

[16] Climate change, in: Impacts, Adaptation, and Vulnerability Part B: Regional Aspects: Working Group II Contribution to the Fifth Assessment Report of the Intergovernmental Panel on Climate Change [Barros, V.R., C.B. Field, D.J. Dokken, M.D. Mastrandrea, K, 2014, p. 688.

[17] G.B.A. Coelho, F.M.A. Henriques, Performance of passive retrofit measures for historic buildings that house artefacts viable for future conditions, Sustain. Cities Soc. 71 (2021), 102982, https://doi.org/10.1016/j.scs.2021.102982.

[18] A report of working group I of the intergovernmental Panel on climate change - summary for policymakers, in: S. Solomon, D. Qin, M. Manning, Z. Chen, M. Marquis, K.B. Averyt, M. Tignor, H.L. Miller (Eds.), Climate Change 2007: the Physical Science Basis. Contribution of Working Group I to the Fourth Assessment Report of the Intergovernmental Panel on Climate Change, Cambridge University Press, Cambridge, United Kingdom and New York, NY, USA, 2007.

[19] Intergovernmental Panel on Climate Change (IPCC), IPCC, 2014, in: R.K. Pachauri, L.A. Meyer (Eds.), Climate Change 2014: Synthesis Report. Contribution of Working Groups I, II and III to the Fifth Assessment Report of the Intergovernmental Panel on Climate Change [Core Writing Team, 2014, p. 151, https://doi.org/10.1017/CBO9781107415324.

[20] IPCC website, Reports, IPCC website - reports. https://www.ipcc.ch/reports/. July 2023.

[21] Climate Change - SPM, Climate Change 2013 – the Physical Science Basis, Cambridge University Press, 2014, https://doi.org/10.1017/CBO9781107415324.

[22] T.F. Stocker, D. Qin, G.-K. Plattner, M. Tignor, S.K. Allen, J. Boschung, A. Nauels, Y. Xia, V. Bex, P.M. Midgley (Eds.), Climate Change 2013: the Physical Science Basis. Contribution of Working Group I to the Fifth Assessment Report of the Intergovernmental Panel on Climate Change (IPCC), Cambridge University Press, Cambridge, United Kingdom and New York, NY, USA, 2013, https://doi.org/10.1017/CBO9781107415324.

[23] M. Kottek, J. Grieser, C. Beck, B. Rudolf, F. Rubel, World Map of the Köppen-Geiger climate classification updated, Meteorol. Z. 15 (2006) 259–263, https://doi.org/10.1127/0941-2948/2006/0130.

[24] G.B.A. Coelho, H.E. Silva, F.M.A. Henriques, Impact of climate change in cultural heritage: from energy consumption to artefacts' conservation and building rehabilitation, Energy Build. 224 (2020), 110250, https://doi.org/10.1016/j.enbuild.2020.110250.

[25] Z. Yu, Y. Song, D. Song, Y. Liu, Spatial interpolation-based analysis method targeting visualization of the indoor thermal environment, Build. Environ. 188 (2021), 107484, https://doi.org/10.1016/j.buildenv.2020.107484.

[26] J. Wu, C. Liu, H. Wang, Analysis of Spatio-temporal patterns and related factors of thermal comfort in subtropical coastal cities based on local climate zones, Build. Environ. 207 (2022), 108568, https://doi.org/10.1016/j.buildenv.2021.108568.

[27] I. Vandemeulebroucke, L. Kotova, S. Caluwaerts, N. Van Den Bossche, Degradation of brick masonry walls in Europe and the Mediterranean: advantages of a response-based analysis to study climate change, Build. Environ. 230 (2023), 109963, https://doi.org/10.1016/j.buildenv.2022.109963.

[28] H. Choi, H. Kim, S. Yeom, T. Hong, K. Jeong, J. Lee, An indoor environmental quality distribution map based on spatial interpolation methods, Build. Environ. 213 (2022), 108880, https://doi.org/10.1016/j.buildenv.2022.108880.

[29] K. Verichev, M. Zamorano, M. Carpio, Assessing the applicability of various climatic zoning methods for building construction: case study from the extreme southern part of Chile, Build. Environ. 160 (2019), 106165, https://doi.org/10.1016/j.buildenv.2019.106165.

[30] M. Rajput, M.R. Gahrooei, G. Augenbroe, A statistical model of the spatial variability of weather for use in building simulation practice, Build. Environ. 206 (2021), 108331, https://doi.org/10.1016/j.buildenv.2021.108331.

[31] G.B.A. Coelho, H.E. Silva, F.M.A. Henriques, Calibrated hygrothermal simulation models for historical buildings, Build. Environ. 142 (2018) 439–450, https://doi.org/10.1016/j.buildenv.2018.06.034.

[32] Z. Huijbregts, M.H.J. Martens, A.W.M. van Schijndel, H.L. Schellen, The use of computer simulation models to evaluate the risks on damage to objects exposed to varying indoor climate conditions in the past, present, and future, in: Proceedings of the 2nd Central European Symposium on Building Physics, 2013, pp. 335–342.

[33] A.W.M.J. van Schijndel, H.L.H. Schellen, Mapping future energy demands for European museums, J. Cult. Herit. 31 (2018) 189–201, https://doi.org/10.1016/j.culher.2017.11.013.

[34] C. Sabbioni, P. Brimblecombe, M. Cassar, The Atlas of Climate Change Impact on European Cultural Heritage: Scientific Analysis and Management Strategies, Anthem Press, 2012.

[35] A. Sardella, E. Palazzi, J. von Hardenberg, C. Del Grande, P.D. De Nuntiis, C. Sabbioni, A. Bonazza, Risk mapping for the sustainable protection of cultural heritage in extreme changing environments, Atmosphere 11 (2020) 1–11, https://doi.org/10.3390/atmos11070700.

[36] J. Leissner, R. Kilian, L. Kotova, D. Jacob, U. Mikolajewicz, T. Broström, J. Ashley-Smith, H.L. Schellen, M. Martens, J. van Schijndel, F. Antretter, M. Winkler, C. Bertolin, D. Camuffo, G. Simeunovic, T. Vyhlídal, Climate for Culture: assessing the impact of climate change on the future indoor climate in historic buildings using simulations, Heritage Science 3 (2015) 38, https://doi.org/10.1186/s40494-015-0067-9.

[37] G.B.A. Coelho, H. Entradas Silva, F.M.A. Henriques, Development of a three-dimensional hygrothermal model of a historic building in WUFI ® Plus vs EnergyPlus, MATEC Web of Conferences 282 (2019), 02079, https://doi.org/10.1051/matecconf/201928202079.

[38] EN ISO 15927-4, Hygrothermal Performance of Buildings - Calculation and Presentation of Climatic Data - Part 4: Hourly Data for Assessing the Annual Energy Use for Heating and Cooling, European Commitee for Standardization (CEN), 2005, p. 16.

[39] A. Skartveit, J.A. Olseth, A model for the diffuse fraction of hourly global radiation, Sol. Energy 38 (1986) 271–274, https://doi.org/10.1016/0038-092X(87)90049-1.

[40] A. Skartveit, J.A. Olseth, M.E. Tuft, An hourly diffuse fraction model with correction for variability and surface albedo, Sol. Energy 63 (1998) 173–183, https://doi.org/10.1016/S0038-092X(98)00067-X.

[41] G.B.A. Coelho, V.P. de Freitas, F.M.A. Henriques, H.E. Silva, Retrofitting historic buildings for future climatic conditions and consequences in terms of artifacts conservation using hygrothermal building simulation, Appl. Sci. 13 (2023) 2382, https://doi.org/10.3390/app13042382.

[42] H.E. Silva, F.M.A. Henriques, Microclimatic analysis of historic buildings: a new methodology for temperate climates, Build. Environ. 82 (2014) 381–387, https://doi.org/10.1016/j.buildenv.2014.09.005.

[43] D. Camuffo, Microclimate for Cultural Heritage: Conservation, Restoration, and Maintenance of Indoor and Outdoor Monuments, second ed., Elsevier, New York, USA, 2014.

[44] F. Antretter, H. Künzel, M. Winkler, M. Pazold, J. Radon, C. Kokolsky, S. Stadler, WUFI®Plus – Fundamentals, 2017.

[45] F.D. Santos, K. Forbes, R. Moita (Eds.), Climate Change in Portugal. Scenarios, Impacts and Adaptation Measures - SIAM Project, Gradiva, Lisbon, Portugal, 2002.

[46] F.D. Santos, P. Miranda (Eds.), Climate Change in Portugal. Scenarios, Impacts and Adaptation Measures - SIAM Project II, 2006 (in Portuguese), Gradiva, Lisboa, Portugal.

[47] ClimAdapPT, Local project. https://eeagrants.org/archive/2009-2014/projects/PT04-0007. July 2023.

[48] https://www.eea.europa.eu/data-and-maps/data/copernicus-land-monitoring-service-eu-dem (accessed on July 2022).

[49] QGIS Development Team, QGIS geographic information system, Available online: https://www.qgis.org. July 2022.

[50] G.B.A. Coelho, D. Kraniotis, A multistep approach for the hygrothermal assessment of a hybrid timber and aluminium based facade system exposed to different sub-climates in Norway, Energy Build. 296 (2023), 113368, https://doi.org/10.1016/j.enbuild.2023.113368.

[51] M. Posani, R. Veiga, V.P. de Freitas, Thermal renders for traditional and historic masonry walls: comparative study and recommendations for hygric compatibility, Build. Environ. 228 (2023), 109737, https://doi.org/10.1016/j.buildenv.2022.109737.

[52] W. Köppen, Klassifikation der Klimate nach Temperatur, Niederschlag und Jahresablauf (Classification of climates according to temperature, precipitation and seasonal cycle), Petermanns Geogr. Mittl. 64 (1918) 193–203.

[53] IPMA, Educational area: climate of Portugal (continental). https://www.ipma.pt/pt/educativa/tempo.clima/index.jsp?page=clima.pt.xml. October 2022.

[54] F.M.A. Henriques, O Clima de Portugal, in: Comportamento Higrotérmico de Edifícios, FCT-UNL, Monte de Caparica, 2013, pp. 285–312.

[55] F.M.A. Henriques, Quantification of wind driven rain. An experimental approach, Build. Res. Inf. 20 (1992) 295–297, https://doi.org/10.1080/09613219208727227.

[56] D.R. Legates, C.J. Willmott, Mean seasonal and spatial variability in global surface air temperature, Theor. Appl. Climatol. 41 (1990) 11–21, https://doi.org/10.1007/BF00866198.

[57] LNEG, Climates-SCE - climatic data for the Portuguese building certification system. https://www.lneg.pt/servicos/328/2263/. January 2020.

[58] IPMA, Climate normals. https://www.ipma.pt/en/oclima/normais.clima/. October 2022.

[59] EN 15757:2010, Conservation of Cultural Property - Specifications for Temperature and Relative Humidity to Limit Climate-Induced Mechanical Damage in Organic Hygroscopic Materials, European Committee for Standardization (CEN), 2010.

[60] J.L. Barros, P.P. Santos, A.O. Tavares, P. Freire, A.B. Fortunato, A. Rilo, F.S.B. F. Oliveira, The complexity of the coastal zone: definition of typologies in Portugal as a contribution to coastal disaster risk reduction and management, Int. J. Disaster Risk Reduc. 86 (2023), 103556, https://doi.org/10.1016/j.ijdrr.2023.103556.

[61] A. Radu, E. Barreiro, H. Saber, H. Hens, J. Vinha, M. Vasilache, M. Bomberg, O. Koronthalyova, P. Matiasovsky, R. Becker, T. Kalamees, V.P. de Freitas, W. Maref, Heat , Air and Moisture Transfer Terminology - Parameters and Concepts, CIB, FEUP, FEUP Edições, Porto, Portugal, 2012.